Received September 2002
Revised May 2003
Accepted May 2003

A new volumetric and shear locking-free 3D enhanced strain element

R.J. Alves de Sousa
Departamento de Engenharia Mecânica, Universidade de Aveiro, Portugal
IDMEC – Faculdade de Engenharia, Universidade do Porto, Portugal
R.M. Natal Jorge
IDMEC – Faculdade de Engenharia, Universidade do Porto, Portugal
R.A. Fontes Valente
Departamento de Engenharia Mecânica, Universidade de Aveiro, Portugal
IDMEC – Faculdade de Engenharia, Universidade do Porto, Portugal
J.M.A. César de Sá
IDMEC – Faculdade de Engenharia, Universidade do Porto, Portugal

Keywords *Shell structures, Strain measurement, Shear strength*

Abstract *This paper focuses on the development of a new class of eight-node solid finite elements, suitable for the treatment of volumetric and transverse shear locking problems. Doing so, the proposed elements can be used efficiently for 3D and thin shell applications. The starting point of the work relies on the analysis of the subspace of incompressible deformations associated with the standard (displacement-based) fully integrated and reduced integrated hexahedral elements. Prediction capabilities for both formulations are defined related to nearly-incompressible problems and an enhanced strain approach is developed to improve the performance of the earlier formulation in this case. With the insight into volumetric locking gained and benefiting from a recently proposed enhanced transverse shear strain procedure for shell applications, a new element conjugating both the capabilities of efficient solid and shell formulations is obtained. Numerical results attest the robustness and efficiency of the proposed approach, when compared to solid and shell elements well-established in the literature.*

Introduction

Several problems of important physical meaning, such as incompressible elasticity, plasticity of metals or, additionally, the flow of certain fluids, involve the inclusion and treatment of the incompressibility phenomenon.

It is worth noting the funding by *Ministério da Ciência e Ensino Superior*, *Fundação para a Ciência e Tecnologia*, Portugal, under grants PRAXIS XXI/BD/21662/99 as well as *FEDER* under grant POCTI/33640/EME/2000. These supports are gratefully acknowledged.

Engineering Computations
Vol. 20 No. 7, 2003
pp. 896-925

0264-4401
DOI 10.1108/02644400310502036

Mathematically, incompressibility modelling relates to the imposition of a constraint over the analysed continuum, enforcing the volumetric part of the strain field to be zero or very small when compared to its deviatoric counterpart. However, the same treatment involving the frame of the finite element method (FEM) imposes some difficulties, in particular, when low-order elements' formulations are employed.

Low-order elements offer simpler implementation when compared with higher-order formulations allowing, at the same time, straightforward mesh operations to be performed. Nevertheless, problems can arise in the presence of incompressibility, as stated before, leading to the so-called volumetric locking phenomenon. In this case, bilinear elements (in two-dimensional analysis) and trilinear solid elements (in three-dimensional analysis) are not able to grant the complete nullity of the volumetric strain. This leads to an overestimation of stiffness values related to the volumetric deformation and, in consequence, to near zero values of displacements obtained.

Several approaches have been proposed in the latest decades to reduce or alleviate volumetric locking occurrence. Reduced and selective reduced integration (SRI) techniques were the first successful irreducible form of solutions for locking problems, although in the beginning not directed specifically to volumetric locking (Hughes *et al.*, 1978; Zienkiewicz *et al.*, 1971). For the particular case of the eight-node hexahedral finite element, both techniques correspond to the use of a lower quadrature rule (one Gauss point, corresponding to the elements' center) in opposition to the so-called complete quadrature rule ($2 \times 2 \times 2$ Gauss points). While the (total) reduced integration appeared to lead to non-physical (spurious) deformation patterns, selective reduced integration proved quite successful, being in some extent the predecessor of the B-bar method (Hughes, 1977). In the latter, shape functions derivatives related to the volumetric part of deformation were replaced by approximations resulting from a mixed formulation, without resorting to reduced integrations.

All these methods proved to be effective proposals in alleviating specifically the volumetric locking, although their performance in bending dominated situations revealed some deficiencies. For selective reduced integration and B-bar cases, in addition, their application is in some extent limited to materials whose strain (stress) tensor can be decomposed into volumetric and deviatoric parts. Other formulations succeeded in using an augmented functional, when compared to that obtained from displacement-based approaches, incorporating additional fields into the formulation and leading to the onset of general mixed methods. For the **u**/**p** mixed formulation, displacements are interpolated with functions providing C^0 continuity requirements, while the pressure field is introduced via discontinuous functions between elements (Hughes, 2000; Zienkiewicz and Taylor, 2000).

In the 1990s, the work of Simo and Rifai (1990) introduced the enhanced strain method. In this formulation, the strain field is enlarged with the inclusion of an extra internal field of variables, resulting therefore in additional deformation modes. A particular choice of the extra modes of deformation led to the QM6 element, derived via the incompatible modes method of Wilson *et al.* (1973), a formulation designed to improve the performance of quadrilateral elements in 2D bending problems (Taylor *et al.*, 1976).

Due to its versatility, the enhanced strain method was successfully applied in 2D, 3D and shell formulations achieving good results even with coarse meshes (Andelfinger and Ramm, 1993; Armero and Dvorkin, 2000; de Borst and Groen, 1999; de Souza Neto *et al.*, 1996; Glaser and Armero, 1997; Kasper and Taylor, 2000; Korelc and Wriggers, 1996; Piltner, 2000; Rohel and Ramm, 1996; Simo and Armero, 1992; Simo and Rifai, 1990; Simo *et al.*, 1993). The possibility of, respecting some conditions, "freely" adding extra variables (deformation modes) represents an important matter, being directly related to a given element's performance.

Concerning near incompressible situations, and specifically for 2D plane strain problems, the number of additional variables to use in reliable volumetric locking-free elements can vary from two to four, as in the proposals of César de Sá and Natal Jorge (1999) or Simo and Rifai (1990) among others. In 3D analysis, this number is still a matter of discussion, varying from 9 to 12 in accordance to Korelc and Wriggers (1996), 12 according to Simo *et al.* (1993) or still 6 to 30, according to Andelfinger and Ramm (1993), only to quote some relevant publications in the field.

Still dealing with hexahedral finite elements, but departing from the exposed before, an interesting application relates to the shell structures modelling. In fact, 3D elements were the starting point of some shell elements, as in the onset of the degenerated approach, with the pioneer work of Ahmad *et al.* (1970). For the proper reproduction of this particular kinematics, either of Mindlin or Kirchhoff-Koiter type, some simplifications were taken, leading to a class of elements incorporating plane-stress assumptions with undesirable losses in the general character provided by full 3D material laws of solid elements.

In this sense, a correct reproduction of shells (and plates) structures behaviour with the use of tridimensional elements is desirable. Apart from the easier formulation and material considerations, solid elements provide a straightforward extension to geometrically non-linear problems, in particular, in the presence of large rotations, once the only degrees of freedom involved are (additive type) translations. Another difficulty in dealing with shell elements is the treatment of corner-like zones (for example, in reinforced shell structures), with the resulting drilling degrees of freedom, and also the treatment of conjunction between solids and shells in the same model.

For a successful modelling of general shells, with no limitations on thickness values, transverse shear locking effects must be accounted. Transverse shear

locking phenomenon relates to the inability of a given element to reproduce a null transverse shear strain energy state in pure bending (César de Sá *et al.*, 2002). Backward in the earlier developments, shear locking in degenerated shell elements were revealed as thickness values tended to small values. The first successful procedures to overcome this artificial behaviour were the cited selective numerical under-integration of the transverse shear strain terms. The appearance of spurious zero energy deformation modes required the development of stabilization or projection techniques in order to recover the correct rank of the stiffness matrices involved (Belytschko *et al.*, 1992). In case the full quadrature is maintained, some procedures proved to be efficient in attenuating transverse shear locking. Among the successful techniques were the so-called mixed interpolation of tensorial (transverse shear strain) components (MITC), from the initial work of Dvorkin and Bathe (1984) and later on Bathe and Dvorkin (1986), Bathe *et al.* (2000), Chapelle and Bathe (2000) and Lee and Bathe (2002).

Additionally, it is also worth noting the assumed natural strain (ANS) approach first introduced by Park (1986) and Park and Stanley (1986). Both formulations employ a set of additional sampling points over a finite element in order to obtain a substitute or complementary strain field leading to the fulfilment of the Kirchhoff-Koiter hypothesis in the thin shell limit. Relating to the MITC, this procedure is usually cast into a more general frame than the conventional degenerated formulation. An example is the "solid-shell" class of elements developed by Doll *et al.* (2000), Harnau and Schweizerhof (2002), Hauptmann and Schweizerhof (1998) and Hauptmann *et al.* (2001). In this formulation, mixed interpolation as described was used for the transverse shear locking, while the EAS method is adopted in attenuating membrane locking. Thickness, volumetric and trapezoidal locking appearance is related to these elements, and proper treatments of the last locking effects are needed in order to reach a successful and general finite element (Harnau and Schweizerhof, 2002).

In this paper, based on the framework of subspace of deformations analysis, already successfully applied in 2D plane strain (César de Sá and Natal Jorge, 1999) and shell problems (César de Sá *et al.*, 2002), a new volumetric and shear locking-free EAS element for 3D analyses is proposed. The main idea is the improvement of the original strain field, in an additive way, leading to elements with higher performance in the presence of volumetric locking (3D applications) and transverse shear locking (shell structures applications).

Volumetric locking – subspace analysis

The incompressibility problem can be formulated as a constrained minimization of a functional (César de Sá and Natal Jorge, 1999). In simple terms, the goal is to obtain, in the linear space of admissible solutions U, a field of displacement $\mathbf{u}$, that minimizes the total energy of the system, located in the

subspace of the incompressible deformations I and simultaneously contained in the space of all the solutions ($I \subset U$). This statement can be posed in the form:

$$I = \{\mathbf{u} \in U: \operatorname{div}(\mathbf{u}) = 0\} \tag{1}$$

In an approach done by the FEM, the linear space of the admissible solutions U, and the respective subspace I, previously defined, are approximated by the spaces U^h and I^h, respectively.

A two field finite element solution can be expressed for linear elasticity, according to César de Sá and Natal Jorge (1999), by:

$$\begin{bmatrix} \mathbf{K} & \mathbf{Q} \\ -\mathbf{Q} & 0 \end{bmatrix} \begin{bmatrix} \mathbf{u}^h \\ \mathbf{p}^h \end{bmatrix} = \begin{bmatrix} \mathbf{f}^h_{\text{ext}} \\ 0 \end{bmatrix} \tag{2}$$

where $\mathbf{f}_{\text{ext}}$ is the vector of applied external forces, $\mathbf{p}$ is the hydrostatic pressure and $\mathbf{K}$ is the stiffness matrix. The superscript (h) means that the variable in cause is a finite element approximation.

The incompressibility condition is given by the second group of equations defined in equation (2),

$$\mathbf{Q}\mathbf{u}^h = 0 \tag{3}$$

which will define the subspace of the incompressible deformations I^h as:

$$I^h = \{\mathbf{u}^h \in U^h: \mathbf{Q}\mathbf{u}^h = 0\} \tag{4}$$

In order to avoid the trivial solution ($\mathbf{u}^h = 0$) in equation (3), the field of displacements $\mathbf{u}^h$ should belong to the nullspace of $\mathbf{Q}$, that is, to the subspace of the incompressible deformations I^h. The approximated displacements $\mathbf{u}^h$ are contained in I^h being therefore, a linear combination of a given basis of I^h elements.

If the subspace I^h is an approach to the original subspace I, it is plausible to admit that it cannot reproduce all the possible solutions contained in I. In fact, different formulations lead to better or worse approximations for the I subspace. The volumetric locking phenomenon occurs when for a certain group of boundary conditions and external forces, applied in a near incompressible situation, the expected solution or some of its components do not appear properly represented in the subspace I^h. Different types of elements can offer distinct subspaces of incompressible deformations, originating therefore different solutions (César de Sá and Owen, 1986).

To characterize the already defined subspace I^h, consider a standard isoparametric eight-node hexahedral element with domain Ω_e (Figure 1). For small deformations, the incompressibility constraint ($\varepsilon_{ii} = 0$) can take the form:

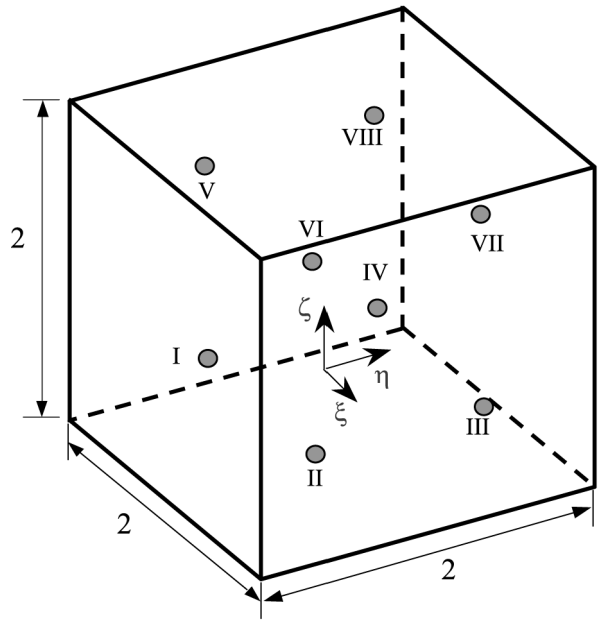

Figure 1.
Standard eight-node isoparametric hexahedral element with $2 \times 2 \times 2$ Gauss points numerical integration rule

$$\int_{\Omega_e} \mathrm{div}(\mathbf{u})\, d\Omega_e = \int_{\Omega_e} \left(\frac{\partial u}{\partial \xi} + \frac{\partial v}{\partial \eta} + \frac{\partial w}{\partial \zeta} \right) d\Omega_e = 0 \tag{5}$$

At the element level, in any point of the domain, the displacement field can be interpolated using the standard linear shape functions (Hughes, 2000; Zienkiewicz and Taylor, 2000):

$$\mathbf{u} \approx \mathbf{u}_e^h = \mathbf{N}(\xi, \eta, \zeta)\mathbf{d}_e \tag{6}$$

One way to guarantee the incompressibility condition is to assure that the integrand function in equation (5) is zero. Substituting equation (6) in equation (5) results:

$$\frac{\partial u}{\partial \xi} + \frac{\partial v}{\partial \eta} + \frac{\partial w}{\partial \zeta} = [N_{i,\xi}(\xi, \eta, \zeta) \quad N_{i,\eta}(\xi, \eta, \zeta) \quad N_{i,\zeta}(\xi, \eta, \zeta)]\, \{\mathbf{d}_e\} = 0 \tag{7}$$

for $i = 1, n_{\mathrm{nodes}}^e$. Making use of a complete integration ($2 \times 2 \times 2$, eight Gauss points, Figure 1), the application of equation (7) leads to,

$$\begin{bmatrix}
-a & -a & -a & a & -c & -c & c & c & -b & -c & a & -c & -c & -c & a & c & -b & c & b & b & b & -b & c & c \\
-a & -c & -c & a & -a & -a & c & a & -c & -c & c & -b & -c & -b & c & c & -c & a & b & c & c & -b & b & b \\
-c & -c & -b & c & -a & -c & a & a & -a & -a & c & -c & -b & -b & b & b & -c & c & c & c & a & -c & b & c \\
-c & -a & -c & c & -c & -b & a & c & -c & -a & a & -a & -b & -c & c & b & -b & b & c & b & c & -c & c & a \\
-c & -c & -a & c & -b & -c & b & b & -b & -b & c & -c & -a & -a & a & a & -c & c & c & c & b & -c & a & c \\
-c & -b & -c & c & -c & -a & b & c & -c & -b & b & -b & -a & -c & c & a & -a & a & c & a & c & -c & c & b \\
-b & -b & -b & b & -c & -c & c & c & -a & -c & b & -c & -c & -c & b & c & -a & c & a & a & a & -a & c & c \\
-b & -c & -c & b & -b & -b & c & b & -c & -c & c & -a & -c & -a & c & c & -c & b & a & c & c & -a & a & a
\end{bmatrix}$$

$$\times \{\mathbf{d}_e\} = \{0\} \tag{8}$$

where the results for each Gauss point are grouped by rows and:

$$a = \frac{1}{8}(1+f)(1+f), \quad b = \frac{1}{8}(1-f)(1-f), \quad c = \frac{1}{8}(1+f)(1-f)$$
$$\text{and} \quad f = \frac{\sqrt{3}}{3} \tag{9}$$

Equation (8) contains a matrix (**Q**) of rank seven. Being 24, the total number of degrees of freedom, i.e. the dimension of the subspace of admissible solutions U^h, there will be a dimension $24-7 = 17$ for the incompressible deformations subspace.

$$\text{rank}(\mathbf{Q}) = 7 \wedge \text{nullity}(\mathbf{Q}) = 17 \tag{10}$$

If, for the same element, a reduced numerical integration scheme with only one Gauss point is used ($\xi = \eta = \zeta = 0$), the imposition of condition (7) will lead to a subspace of dimension 23, when the maximum dimension of the space of the admissible solutions is 24. The matrix in equation (8) is rewritten as follows,

$$\frac{1}{8}\begin{bmatrix} -1 & -1 & -1 & 1 & -1 & -1 & 1 & 1 & -1 & -1 & 1 & -1 & -1 & -1 & 1 & 1 & -1 & 1 & 1 & 1 & 1 & -1 & 1 & 1 \end{bmatrix}$$

$$\times \{\mathbf{d}_e\} = \{0\} \tag{11}$$

and

$$\text{rank}(\mathbf{Q}) = 1 \wedge \text{nullity}(\mathbf{Q}) = 23 \quad (12)$$

Analysing these two possible bases for the subspace of the incompressible deformations, it can be inferred clearly that the use of the reduced integration allows the reproduction of more six incompressible displacement modes than the case of complete integration. Since the admissible incompressible solutions are nothing more than a linear combination of a given I^h basis, this can be a quite reasonable explanation for the good performance of the reduced integration techniques in volumetric locking problems, and why the classical complete integration numerical integration locks.

For a clear illustration of the last statements, a graphical representation of the linearly independent elements which form the basis of the incompressible deformations subspace is shown in Figure 2. The six rigid body motions can be obtained linearly combining these elements. The displacement field associated with each mode is plotted in Table I. The modes 1-17 are reproduced both by the complete and the reduced integration. The modes 18-23 are reproduced only by the reduced integration, being volumetric locking situations for the complete integration. They can be divided into four main groups:

(1) simple edges translations, in *x, y* and *z* directions, represented by the modes 1-12;

(2) expansion/contraction of one face, modes 13-17;

(3) hourglass modes, 18-20;

(4) warping modes, 21-23.

In the following sections, the proposed approaches to alleviate locking effects (using the enhanced strain method) are conveniently defined within the subspace analysis framework just described.

Formulation of volumetric and transverse shear locking-free elements

As already referred, the reduced integration, selective reduced integration and similar techniques have proved to be efficient methods on attenuating the volumetric locking. However, the behaviour in bending dominated situations is not the best, and for the case of the SRI techniques, the analysis is in some measure limited to materials where the stress tensor allows the decomposition in volumetric and deviatoric components.

On the other hand, the enhanced strain method is a powerful technique, in the sense that permits the inclusion of more or less additional variables for the enhanced strain field. Thus, it is possible to construct a formulation with good behaviour both in near incompressible situation and bending situations.

However, the number of additional variables in the enhanced field is a crucial matter. If increasing the number of additional variables, and

consequently, modes of deformation, normally improves the element's performance, it can also lead to instabilities, numerical inefficiency and large CPU costs. Using the classical complete (eightw Gauss points) numerical integration, the objective turns therefore to reach the dimension 23 for the subspace of incompressible deformations. It was already shown

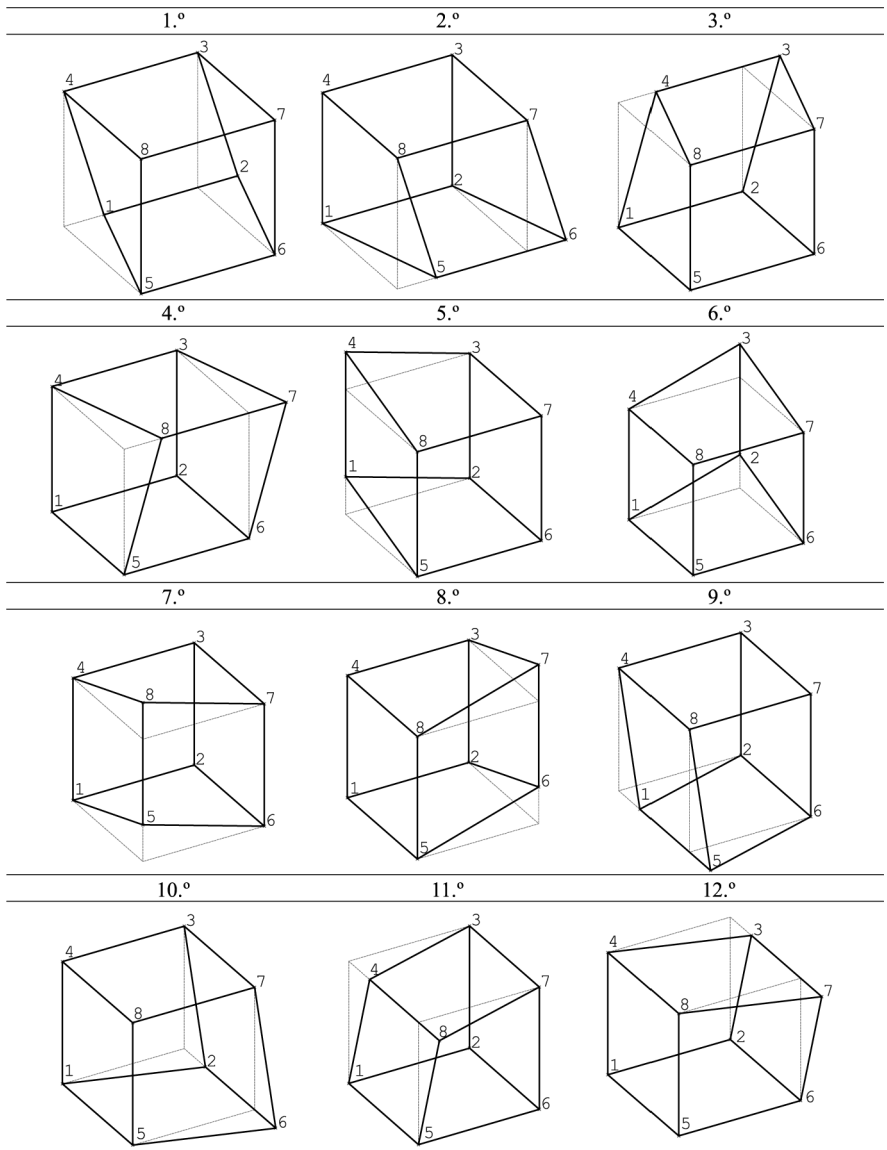

Figure 2.
Basic components of the incompressible deformations subspace

(*continued*)

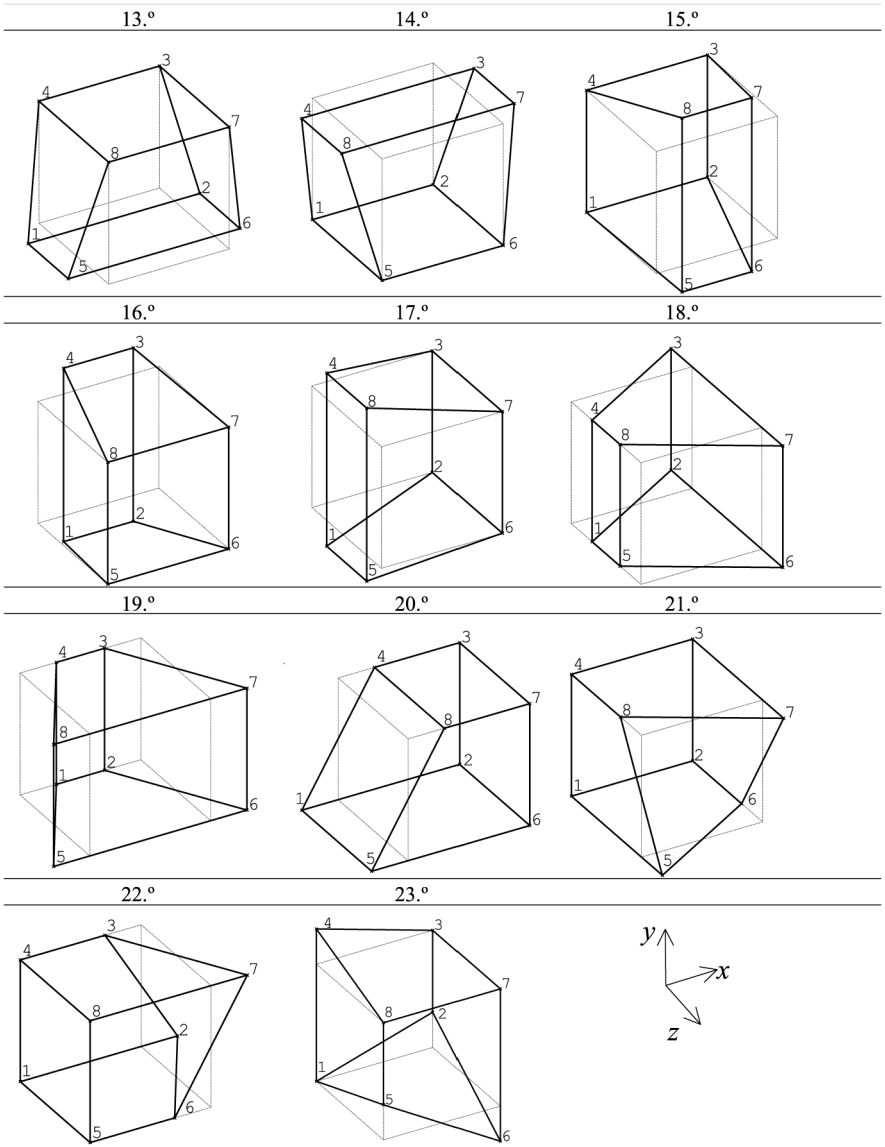

Figure 2.

(Alves de Sousa *et al.*, 2002) that this subspace dimension is related to a good performance in 3D volumetric locking situations.

At the element level, the interpolation of the strain field follows the usual methodology (Simo and Rifai, 1990),

$\mathbf{m} = \{u_{=1}$	v_1	w_1	u_2	v_2	w_2	u_3	v_3	w_3	u_4	v_4	w_4	u_5	v_5	w_5	u_6	v_6	w_6	u_7	v_7	w_7	u_8	v_8	$w_8\}^{\mathrm{T}}$
$\mathbf{m}_1 = \{1$	0	0	1	0	0	0	0	0	0	0	0	0	0	0	0	0	0	0	0	0	0	0	$0\}^{\mathrm{T}}$
$\mathbf{m}_2 = \{0$	0	0	0	0	0	0	0	0	0	0	0	0	0	0	1	0	0	0	0	0	0	0	$0\}^{\mathrm{T}}$
$\mathbf{m}_3 = \{0$	0	0	0	0	0	1	0	0	1	0	0	0	0	0	0	0	0	0	0	0	0	0	$0\}^{\mathrm{T}}$
$\mathbf{m}_4 = \{0$	0	0	0	0	0	0	0	0	0	0	0	0	0	0	0	0	0	1	0	0	1	0	$0\}^{\mathrm{T}}$
$\mathbf{m}_5 = \{0$	1	0	0	0	0	0	0	0	0	1	0	0	0	0	0	0	0	0	0	0	0	0	$0\}^{\mathrm{T}}$
$\mathbf{m}_6 = \{0$	0	0	0	1	0	0	1	0	0	0	0	0	0	0	0	0	1	0	0	0	0	0	$0\}^{\mathrm{T}}$
$\mathbf{m}_7 = \{0$	0	0	0	0	0	0	0	0	0	0	0	0	1	0	0	0	0	0	0	0	0	1	$0\}^{\mathrm{T}}$
$\mathbf{m}_8 = \{0$	0	0	0	0	0	0	0	0	0	0	0	0	0	0	0	1	0	0	1	0	0	0	$0\}^{\mathrm{T}}$
$\mathbf{m}_9 = \{0$	0	1	0	0	0	0	0	0	0	0	0	0	0	1	0	0	0	0	0	0	0	0	$0\}^{\mathrm{T}}$
$\mathbf{m}_{10} = \{0$	0	0	0	0	1	0	0	0	0	0	0	0	0	0	0	0	1	0	0	0	0	0	$0\}^{\mathrm{T}}$
$\mathbf{m}_{11} = \{0$	0	0	0	0	0	0	0	0	0	0	1	0	0	0	0	0	0	0	0	0	0	0	$1\}^{\mathrm{T}}$
$\mathbf{m}_{12} = \{0$	0	0	0	0	0	0	0	1	0	0	0	0	0	0	0	0	0	0	0	1	0	0	$0\}^{\mathrm{T}}$
$\mathbf{m}_{13} = \{-1$	0	1	1	0	1	0	0	0	0	0	0	0	0	0	0	0	-1	0	0	0	0	0	$0\}^{\mathrm{T}}$
$\mathbf{m}_{14} = \{0$	0	0	1	0	0	1	0	1	-1	0	1	-1	0	-1	1	0	0	1	0	-1	-1	0	$-1\}^{\mathrm{T}}$
$\mathbf{m}_{15} = \{0$	0	0	0	0	0	0	0	0	0	0	0	1	-1	0	-1	-1	0	-1	1	0	1	1	$0\}^{\mathrm{T}}$
$\mathbf{m}_{16} = \{1$	-1	0	-1	-1	0	-1	1	0	1	1	0	0	0	0	0	0	0	0	0	0	0	0	$0\}^{\mathrm{T}}$
$\mathbf{m}_{17} = \{0$	-1	1	0	0	0	0	0	0	0	1	1	0	-1	-1	0	0	0	0	0	0	0	1	$-1\}^{\mathrm{T}}$
$\mathbf{m}_{18} = \{0$	0	1	0	0	-1	0	0	-1	0	0	1	0	0	-1	0	0	1	0	0	1	0	0	$-1\}^{\mathrm{T}}$
$\mathbf{m}_{19} = \{1$	0	0	-1	0	0	-1	0	0	1	0	0	-1	0	0	1	0	0	1	0	0	-1	0	$0\}^{\mathrm{T}}$
$\mathbf{m}_{20} = \{-1$	0	0	0	0	0	-1	0	0	0	0	0	-1	0	0	0	0	0	0	0	0	1	0	$0\}^{\mathrm{T}}$
$\mathbf{m}_{21} = \{0$	0	0	0	0	0	0	0	0	0	0	0	0	0	1	0	0	-1	0	0	1	0	0	$-1\}^{\mathrm{T}}$
$\mathbf{m}_{22} = \{0$	0	0	1	0	0	-1	0	0	0	0	0	0	0	0	-1	0	0	1	0	0	0	0	$0\}^{\mathrm{T}}$
$\mathbf{m}_{23} = \{0$	0	0	0	1	0	0	0	0	0	1	0	0	1	0	0	-1	0	0	0	0	0	0	$0\}^{\mathrm{T}}$

Table I.
Basic components of the incompressible deformations subspace

$$\varepsilon = \varepsilon_d + \varepsilon_\alpha = \begin{bmatrix} \mathbf{B}_d^e & \mathbf{B}_\alpha^e \end{bmatrix} \begin{bmatrix} \mathbf{d}^e \\ \alpha^e \end{bmatrix} = \hat{\mathbf{B}}^e \hat{\mathbf{d}}^e \tag{13}$$

where $\mathbf{B}_d^e$ is the standard FEM strain-displacement differential operator, function of the standard FEM linear shape functions (Hughes, 2000; Zienkiewicz and Taylor, 2000), while $\mathbf{B}_\alpha^e$ is the one used for the enhanced variables field (α).

At the element level, the operator $\mathbf{B}_\alpha^e$ is previously formulated in the isoparametric space, leading to the $\mathbf{M}_\alpha^e$ matrix. The transition from the isoparametric space to the global reference frame must be carried out very carefully, in order to satisfy the patch test for arbitrary configurations, as stated by Taylor *et al.* (1976),

$$\int_\Omega \mathbf{M}_\alpha \, d\Omega = 0 \tag{14}$$

Condition (14) can also be obtained from the orthogonality condition between the stress field and the enhanced strain field (Simo and Rifai, 1990).

In problems involving distorted meshes, the transition of the differential operator for the enhanced field is also a crucial matter and can have a relevant influence in the element's performance. Following the work of Andelfinger and Ramm (1993), and Simo and Rifai (1990) the transformation provided by equation (15), performed at the center of each finite element, allows the fulfillment of equation (14) by the elements proposed, and can be stated as follows:

$$\mathbf{B}_\alpha^e = \frac{|\mathbf{J}_0|}{|\mathbf{J}|} \mathbf{T}_0 \mathbf{M}_\alpha^e \tag{15}$$

and as usual

$$\mathbf{J} = \begin{bmatrix} \frac{\partial x}{\partial \xi} & \frac{\partial y}{\partial \xi} & \frac{\partial z}{\partial \xi} \\ \frac{\partial x}{\partial \eta} & \frac{\partial y}{\partial \eta} & \frac{\partial z}{\partial \eta} \\ \frac{\partial x}{\partial \zeta} & \frac{\partial y}{\partial \zeta} & \frac{\partial z}{\partial \zeta} \end{bmatrix} \tag{16}$$

$|\mathbf{J}_0|$ and $|\mathbf{J}|$ being Jacobian matrix determinants and α the number of additional variables. The subscript (0) refers to evaluations in the centre of the standard element, ($\xi = \eta = \zeta = 0$). $\mathbf{T}$ is the transformation tensor relating the isoparametric space and the global reference frame, defined by

$$\mathbf{T} = \begin{bmatrix} J_{11}^{-1}J_{11}^{-1} & J_{12}^{-1}J_{12}^{-1} & J_{13}^{-1}J_{13}^{-1} & J_{11}^{-1}J_{12}^{-1} & J_{11}^{-1}J_{13}^{-1} & J_{12}^{-1}J_{13}^{-1} \\ J_{21}^{-1}J_{21}^{-1} & J_{22}^{-1}J_{22}^{-1} & J_{23}^{-1}J_{23}^{-1} & J_{21}^{-1}J_{22}^{-1} & J_{21}^{-1}J_{23}^{-1} & J_{22}^{-1}J_{23}^{-1} \\ J_{31}^{-1}J_{31}^{-1} & J_{32}^{-1}J_{32}^{-1} & J_{33}^{-1}J_{33}^{-1} & J_{31}^{-1}J_{32}^{-1} & J_{31}^{-1}J_{33}^{-1} & J_{32}^{-1}J_{33}^{-1} \\ 2J_{11}^{-1}J_{21}^{-1} & 2J_{12}^{-1}J_{22}^{-1} & 2J_{13}^{-1}J_{23}^{-1} & (J_{11}^{-1}J_{22}^{-1}) + (J_{12}^{-1}J_{21}^{-1}) & (J_{11}^{-1}J_{23}^{-1}) + (J_{21}^{-1}J_{13}^{-1}) & (J_{12}^{-1}J_{23}^{-1}) + (J_{22}^{-1}J_{13}^{-1}) \\ 2J_{11}^{-1}J_{31}^{-1} & 2J_{12}^{-1}J_{32}^{-1} & 2J_{13}^{-1}J_{33}^{-1} & (J_{11}^{-1}J_{32}^{-1}) + (J_{12}^{-1}J_{31}^{-1}) & (J_{11}^{-1}J_{33}^{-1}) + (J_{31}^{-1}J_{13}^{-1}) & (J_{12}^{-1}J_{33}^{-1}) + (J_{32}^{-1}J_{13}^{-1}) \\ 2J_{21}^{-1}J_{31}^{-1} & 2J_{22}^{-1}J_{32}^{-1} & 2J_{23}^{-1}J_{33}^{-1} & (J_{21}^{-1}J_{32}^{-1}) + (J_{22}^{-1}J_{31}^{-1}) & (J_{21}^{-1}J_{33}^{-1}) + (J_{31}^{-1}J_{23}^{-1}) & (J_{22}^{-1}J_{33}^{-1}) + (J_{32}^{-1}J_{23}^{-1}) \end{bmatrix} \tag{17}$$

where J_{ij}^{-1} relates to the ij components of the inverse Jacobian matrix. This expression comes from considering a transformation between two general curvilinear (convective) referentials (Bathe, 1996).

The starting point for the following developments is to include nine additional variables in the enhanced strain field, each one associated with the space derivatives of the displacement field, **H**. Thus, for a 3D problem, the displacement gradient matrix is augmented as follows:

$$\mathbf{H} = \begin{bmatrix} \frac{\partial u}{\partial x} & \frac{\partial u}{\partial y} & \frac{\partial u}{\partial z} \\ \frac{\partial v}{\partial x} & \frac{\partial v}{\partial y} & \frac{\partial v}{\partial z} \\ \frac{\partial z}{\partial x} & \frac{\partial z}{\partial y} & \frac{\partial z}{\partial z} \end{bmatrix} + \begin{bmatrix} \frac{\partial \tilde{u}}{\partial x} & \frac{\partial \tilde{u}}{\partial y} & \frac{\partial \tilde{u}}{\partial z} \\ \frac{\partial \tilde{v}}{\partial x} & \frac{\partial \tilde{v}}{\partial y} & \frac{\partial \tilde{v}}{\partial z} \\ \frac{\partial \tilde{z}}{\partial x} & \frac{\partial \tilde{z}}{\partial y} & \frac{\partial \tilde{z}}{\partial z} \end{bmatrix} \tag{18}$$

Making use of a bubble function N_α,

$$N_\alpha = \frac{1}{2}(1-\xi^2)(1-\eta^2)(1-\zeta^2), \tag{19}$$

extra compatible modes of deformation are added, with the goal of reaching dimension 23 for the subspace $I^h$and resulting in the enhanced strain field interpolation matrix, denoted by $\mathbf{M}_9^e$, defined in the local referential. This increases the total elementary degrees of freedom number from 24 to 33.

$$\mathbf{M}_9^e = \begin{bmatrix} \frac{\partial N_\alpha}{\partial \xi} & 0 & 0 & 0 & 0 & 0 & 0 & 0 & 0 \\ 0 & \frac{\partial N_\alpha}{\partial \eta} & 0 & 0 & 0 & 0 & 0 & 0 & 0 \\ 0 & 0 & \frac{\partial N_\alpha}{\partial \zeta} & 0 & 0 & 0 & 0 & 0 & 0 \\ 0 & 0 & 0 & \frac{\partial N_\alpha}{\partial \xi} & \frac{\partial N_\alpha}{\partial \eta} & 0 & 0 & 0 & 0 \\ 0 & 0 & 0 & 0 & 0 & \frac{\partial N_\alpha}{\partial \xi} & \frac{\partial N_\alpha}{\partial \zeta} & 0 & 0 \\ 0 & 0 & 0 & 0 & 0 & 0 & 0 & \frac{\partial N_\alpha}{\partial \eta} & \frac{\partial N_\alpha}{\partial \zeta} \end{bmatrix} \tag{20}$$

The subsequent transformation to the global frame follows the rule stated in equation (15). This time, the application of equation (7) employs the matrix $\hat{\mathbf{B}}^e$,

$$\hat{\mathbf{B}}^e = [\, \mathbf{B}_d^e \quad \mathbf{B}_9^e \,], \tag{21}$$

and results in the following matrix:

$$\begin{bmatrix} & \begin{matrix} d & d & d & 0 & 0 & 0 & 0 & 0 & 0 \\ -d & d & d & 0 & 0 & 0 & 0 & 0 & 0 \\ -d & -d & d & 0 & 0 & 0 & 0 & 0 & 0 \\ d & -d & d & 0 & 0 & 0 & 0 & 0 & 0 \\ d & d & -d & 0 & 0 & 0 & 0 & 0 & 0 \\ -d & d & -d & 0 & 0 & 0 & 0 & 0 & 0 \\ -d & -d & -d & 0 & 0 & 0 & 0 & 0 & 0 \\ d & -d & -d & 0 & 0 & 0 & 0 & 0 & 0 \end{matrix} \end{bmatrix} \{\hat{\mathbf{d}}_e\} = \{0\} \tag{22}$$

[equation (8)] ⋯

where

$$d = f(1 - f^2)^2 \text{ and } f = \frac{\sqrt{3}}{3} \tag{23}$$

and:

$$\text{rank}(\mathbf{Q}) = 7 \wedge \text{nullity}(\mathbf{Q}) = 26 \tag{24}$$

Following the methodology applied in the subspace analysis for the complete and reduced integration schemes of the previous section, it is possible to conclude that expression (22) will implicitly define a basis for the subspace of incompressible deformations with dimension 20. This value comes from considering a number of 24 + 9= 33 degrees of freedom, subtracting the rank of $\mathbf{Q}$ and the number of null displacement modes associated with the null columns in equation (22) (resulting in a dimension of 33 − 7 − 6 = 20). Note that these

six neglected modes respect the incompressibility condition but concern only non-zero values for the enhanced variables field, not introducing additional displacement modes. This approximated basis can be represented by the first 20 elements represented in Figure 2.

However, the previous approach still achieve less three displacement modes than the use of the reduced integration, which may be the cause of volumetric locking problems for this element (Alves de Sousa *et al.*, 2002).

Hence, three more new internal variables will be added, aiming to be able to reproduce all the modes of Figure 2, which is effectively achieved. At the same time, these new variables, in this case bilinear terms coming from the double derivatives in equation (25) assure the condition of incompressibility as stated by de Borst and Groen (1999), Korelc and Wriggers (1996) and Simo *et al.* (1993).

Focusing only on the volumetric components of the strain field, the modification is performed in the volumetric components of the enhanced field interpolation matrix, this time called $\mathbf{M}_{12}^{e}$,

$$\mathbf{M}_{12}^{e} = \begin{bmatrix} & \dfrac{\partial^2 N_\alpha}{\partial\xi\partial\eta} & \dfrac{\partial^2 N_\alpha}{\partial\xi\partial\zeta} & \dfrac{\partial^2 N_\alpha}{\partial\eta\partial\zeta} \\ & \dfrac{\partial^2 N_\alpha}{\partial\xi\partial\eta} & \dfrac{\partial^2 N_\alpha}{\partial\xi\partial\zeta} & \dfrac{\partial^2 N_\alpha}{\partial\eta\partial\zeta} \\ [\mathbf{M}_9^{e}] & \dfrac{\partial^2 N_\alpha}{\partial\xi\partial\eta} & \dfrac{\partial^2 N_\alpha}{\partial\xi\partial\zeta} & \dfrac{\partial^2 N_\alpha}{\partial\eta\partial\zeta} \\ & 0 & 0 & 0 \\ & 0 & 0 & 0 \\ & 0 & 0 & 0 \end{bmatrix} \tag{25}$$

Replacing $\mathbf{M}_9^{e}$ by $\mathbf{M}_{12}^{e}$ in equation (21) and again applying equation (7) results in

$$\begin{bmatrix} & d & d & d & 0 & 0 & 0 & 0 & 0 & 0 & e & e & e \\ & -d & d & d & 0 & 0 & 0 & 0 & 0 & 0 & -e & e & -e \\ & -d & -d & d & 0 & 0 & 0 & 0 & 0 & 0 & e & -e & -e \\ & d & -d & d & 0 & 0 & 0 & 0 & 0 & 0 & -e & -e & e \\ [\text{equation (8)}] \cdots & d & d & -d & 0 & 0 & 0 & 0 & 0 & 0 & e & -e & -e \\ & -d & d & -d & 0 & 0 & 0 & 0 & 0 & 0 & -e & -e & e \\ & -d & -d & -d & 0 & 0 & 0 & 0 & 0 & 0 & e & e & e \\ & d & -d & -d & 0 & 0 & 0 & 0 & 0 & 0 & -e & e & -e \end{bmatrix} \tag{26}$$

$$\times \{\hat{\mathbf{d}}_e\} = \{0\}$$

where

$$e = f^2 + 1 \text{ and } f = \frac{\sqrt{3}}{3} \tag{27}$$

This will generate an approximation for the subspace of incompressible deformations with dimension 23 (comes from $36-7-6$), again neglecting the modes associated with the six internal degrees of freedom in equation (26), as well in equation (22), which have zero nodal displacements. This fulfils the necessary subspace dimension for a volumetric locking-free element.

The HCiS18 element

Once the requirements for a volumetric locking-free formulation are satisfied, we turn back to the transverse shear locking. Indeed, the two last elements show strong sensitivity to the shear locking phenomenon in problems involving thin shells or plates, with low length to thickness ratio (Alves de Sousa *et al.*, 2002).

Working only in the shear part of the strain field to guarantee the same volumetric locking-free properties already achieved by the use of $\mathbf{M}^{e}_{12}$, an optimal choice of six new enhanced shear modes is added, resulting in the $\mathbf{M}^{e}_{18}$ interpolation matrix, once again function of the bubble function (19).

$$\mathbf{M}^{e}_{18} = \begin{bmatrix} & 0 & 0 & 0 & 0 & 0 & 0 \\ & 0 & 0 & 0 & 0 & 0 & 0 \\ & 0 & 0 & 0 & 0 & 0 & 0 \\ [\mathbf{M}^{e}_{12}] & \dfrac{\partial^2 N_\alpha}{\partial\xi\partial\zeta} & \dfrac{\partial^2 N_\alpha}{\partial\eta\partial\zeta} & 0 & 0 & 0 & 0 \\ & 0 & 0 & \dfrac{\partial^2 N_\alpha}{\partial\xi\partial\eta} & \dfrac{\partial^2 N_\alpha}{\partial\eta\partial\zeta} & 0 & 0 \\ & 0 & 0 & 0 & 0 & \dfrac{\partial^2 N_\alpha}{\partial\xi\partial\eta} & \dfrac{\partial^2 N_\alpha}{\partial\xi\partial\zeta} \end{bmatrix} \tag{28}$$

This element satisfied the patch test (14), and showed a good behaviour in volumetric and transverse shear locking-free related problems, even with distorted meshes (Alves de Sousa *et al.*, 2002).

A new approach: the HCiS12 element

In an alternative approach, it is possible to split the already defined $\mathbf{M}^{e}_{18}$ (equation (28)) matrix into two different ones. The $\mathbf{M}^{e}_{VL}$ matrix, grouping only the enhanced modes related to the volumetric part, and the $\mathbf{M}^{e}_{TSL}$ matrix, referring to the transverse shear enhanced modes.

$$\mathbf{M}_{\mathrm{VL}}^{\mathrm{e}} = \begin{bmatrix} \frac{\partial N_\alpha}{\partial \xi} & 0 & 0 & \frac{\partial^2 N_\alpha}{\partial \xi \partial \eta} & \frac{\partial^2 N_\alpha}{\partial \xi \partial \zeta} & \frac{\partial^2 N_\alpha}{\partial \eta \partial \zeta} \\ 0 & \frac{\partial N_\alpha}{\partial \eta} & 0 & \frac{\partial^2 N_\alpha}{\partial \xi \partial \eta} & \frac{\partial^2 N_\alpha}{\partial \xi \partial \zeta} & \frac{\partial^2 N_\alpha}{\partial \eta \partial \zeta} \\ 0 & 0 & \frac{\partial N_\alpha}{\partial \zeta} & \frac{\partial^2 N_\alpha}{\partial \xi \partial \eta} & \frac{\partial^2 N_\alpha}{\partial \xi \partial \zeta} & \frac{\partial^2 N_\alpha}{\partial \eta \partial \zeta} \\ 0 & 0 & 0 & 0 & 0 & 0 \\ 0 & 0 & 0 & 0 & 0 & 0 \\ 0 & 0 & 0 & 0 & 0 & 0 \end{bmatrix} \tag{29}$$

$$\mathbf{M}_{\mathrm{TSL}}^{\mathrm{e}} = \begin{bmatrix} 0 & 0 & 0 & 0 & 0 & 0 & 0 & 0 & 0 & 0 & 0 & 0 \\ 0 & 0 & 0 & 0 & 0 & 0 & 0 & 0 & 0 & 0 & 0 & 0 \\ 0 & 0 & 0 & 0 & 0 & 0 & 0 & 0 & 0 & 0 & 0 & 0 \\ \frac{\partial N_\alpha}{\partial \xi} & \frac{\partial N_\alpha}{\partial \eta} & 0 & 0 & 0 & 0 & \frac{\partial^2 N_\alpha}{\partial \xi \partial \zeta} & \frac{\partial^2 N_\alpha}{\partial \eta \partial \zeta} & 0 & 0 & 0 & 0 \\ 0 & 0 & \frac{\partial N_\alpha}{\partial \xi} & \frac{\partial N_\alpha}{\partial \zeta} & 0 & 0 & 0 & 0 & \frac{\partial^2 N_\alpha}{\partial \xi \partial \eta} & \frac{\partial^2 N_\alpha}{\partial \eta \partial \zeta} & 0 & 0 \\ 0 & 0 & 0 & 0 & \frac{\partial N_\alpha}{\partial \eta} & \frac{\partial N_\alpha}{\partial \zeta} & 0 & 0 & 0 & 0 & \frac{\partial^2 N_\alpha}{\partial \xi \partial \eta} & \frac{\partial^2 N_\alpha}{\partial \xi \partial \zeta} \end{bmatrix} \tag{30}$$

The use of the $\mathbf{M}_{\mathrm{VL}}^{\mathrm{e}}$ matrix is sufficient to reach the stated dimension for the incompressible deformations subspace in a volumetric locking-free element, i.e. 23. In fact, comparing with equation (26) the only difference when applying equation (30) in equation (7) is the elimination of the six null columns in equations (22) and (26), resulting in this case:

$$\mathrm{rank}(\mathbf{Q}) = 7 \wedge \mathrm{nullity}(\mathbf{Q}) = 23 \tag{31}$$

Consequently, the number of elements in this basis of the incompressible deformations subspace is equal to the nullity of $\mathbf{Q}$ matrix, 23, since there is no need to neglect the six displacement modes related to null nodal displacements.

Referring to the work of César de Sá *et al.* (2002) and Fontes Valente *et al.* (2002) the framework of the subspace analysis can be used to achieve a shear locking-free element. In fact, it is possible to enforce the nullity of the transverse shear strain energy by including, in an additive way, an enhanced strain field directly over the transverse shear strain terms of the original

bilinear degenerated element. This inclusion involves the use of six additional variables per finite element and relies on the analysis of the components of the null transverse shear strain subspace. This new strain-displacement differential operator ($\mathbf{M}^{e}_{TSL}*$) involves derivatives of bubble function (19), being defined as follows:

$$\mathbf{M}^{e}_{TSL}* = \begin{bmatrix} 0 & 0 & 0 & 0 & 0 & 0 \\ 0 & 0 & 0 & 0 & 0 & 0 \\ 0 & 0 & 0 & 0 & 0 & 0 \\ 0 & 0 & 0 & 0 & 0 & 0 \\ \dfrac{\partial N_\alpha}{\partial \xi} & \dfrac{\partial N_\alpha}{\partial \eta} & \dfrac{\partial^2 N_\alpha}{\partial \xi \partial \eta} & 0 & 0 & 0 \\ 0 & 0 & 0 & \dfrac{\partial N_\alpha}{\partial \xi} & \dfrac{\partial N_\alpha}{\partial \eta} & \dfrac{\partial^2 N_\alpha}{\partial \xi \partial \eta} \end{bmatrix} \tag{32}$$

Thus, the crucial idea of the HCiS12 element consists of replacing the enhanced strain field interpolation matrix $\mathbf{M}^{e}_{TSL}$ for the $\mathbf{M}^{e}_{TSL}*$ matrix. This is performed maintaining the volumetric enhanced strain interpolation matrix, $\mathbf{M}^{e}_{VL}$, in order to assure the fulfilment of the incompressible subspace requirements. The result is a new element with 12 additional variables,

$$\mathbf{M}^{e}_{HCiS12} = \begin{bmatrix} \mathbf{M}^{e}_{VL} & \mathbf{M}^{e}_{TSL}* \end{bmatrix} \tag{33}$$

In summary, the proposed HCiS12 element consists of an improvement of the HCiS18 element. In fact, as will be confirmed in the next section, their performances are very close. However, the HCiS12 has the clear advantage of using less six variables in its enhanced strain field, which means more numerical stability and less CPU costs.

Assessments

The goal of the following linear elastic assessments is to test the proposed formulation (HCiS12) performance in situations involving the volumetric locking and/or the transverse shear locking. The sensitivity to mesh distortions is also studied. Comparisons with other formulations are carried out, including:

Solids

- Q1 – classical FEM eight-node hexahedral element with complete integration;
- QM1/E12 – 3D eight-node hexahedral element with 12 internal variables proposed by Simo *et al.* (1993);

- QS/E9 – 3D eight-node hexahedral element with nine internal variables and stabilization proposed by Korelc and Wriggers (1996);
- 3D.EAS-21 – 3D eight-node hexahedral element with 21 internal variables proposed by Andelfinger and Ramm (1993);
- HEXDS – multiple quadrature under-integrated 3D eight-node hexahedral element proposed by Liu *et al.* (1998);
- H1/ME9 – mixed-enhanced eight-node hexahedral element with nine enhanced modes, and complete quadrature rule, proposed by Kasper and Taylor (2000); and
- HCiS18 – 3D eight-node hexahedral element with 18 internal variables proposed by Alves de Sousa *et al.* (2002).

Shells

- SIMO_89 – bilinear shell mixed element for membrane and bending stresses, proposed by Simo *et al.* (1989);
- S4E6P7 – shell element using enhanced transverse shear strain terms, proposed by César de Sá *et al.* (2002);
- MITC4 – fully integrated and mixed interpolated bilinear shell element derived by Dvorkin and Bathe (1984);
- EAS7-ANS – in plane bilinear enhanced shell element proposed by Andelfinger and Ramm (1993);
- QPH – quadrilateral shell element with physical hourglass control proposed by Belytschko and Leviathan (1994).

Clamped square plate with concentrated load

Figure 3 shows a clamped square plate, loaded by a concentrated load F. One quarter of the geometry needs to be analysed, using meshes of 2×2 and 4×4 elements. The plotted results for vertical displacement in the loaded point are normalized against the analytical solution (Table II) of Kirchhoff plate theory.

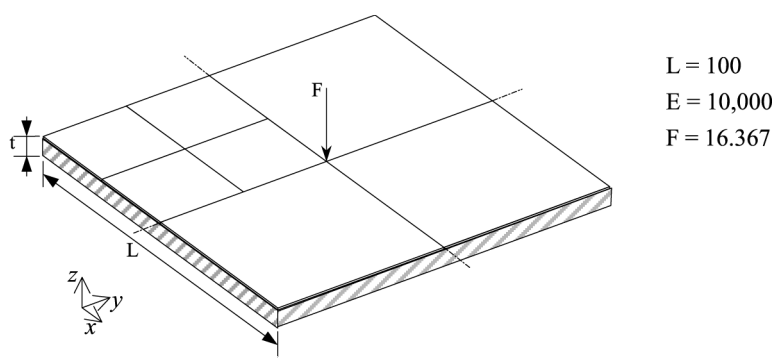

Figure 3.
Clamped square plate under concentrated load (2×2 mesh)

Poisson's coefficient values for compressible and near-incompressible behaviours as well as low length to thickness ratios (1/100 and 1/1,000) are studied.

The proposed solid elements perform well even in situations of near incompressibility allied to low length to thickness ratios, where volumetric and transverse shear locking are expected. The accuracy is as good as for the shell element.

Block under compression

This well-known test aims to assess the performance of the elements in near incompressibility situations allied to mesh distortions (Andelfinger and Ramm, 1993). Figure 4 shows a block of dimensions $100 \times 100 \times 50$, with near incompressibility properties, subjected to a distributed load, in its central area of 20×20. By symmetry, only one quarter of the model is studied, using two different meshes of $5 \times 5 \times 5$ elements: a regular one

		0.3					0.4999[b]		
	Mesh	HCiS12	HCiS18	S4E6P7	MITC4[a]	EAS7-ANS	HCiS12	HCiS18	S4E6P7
$t/L =$ 1/100	2×2	0.869	0.884	0.869	0.868	0.889	0.875	0.885	0.875
	4×4	0.970	0.974	0.971	0.969	0.976	0.973	0.976	0.974
$t/L =$ 1/1,000	2×2	0.866	0.882	0.866	NA	NA	0.868	0.879	0.870
	4×4	0.966	0.972	0.966	NA	NA	0.968	0.972	0.968

Notes: [a]From Andelfinger and Ramm (1993); [b]not available for the MITC4 and EAS7-ANS elements; NA – not available.

Table II. Normalized displacements for the clamped square plate

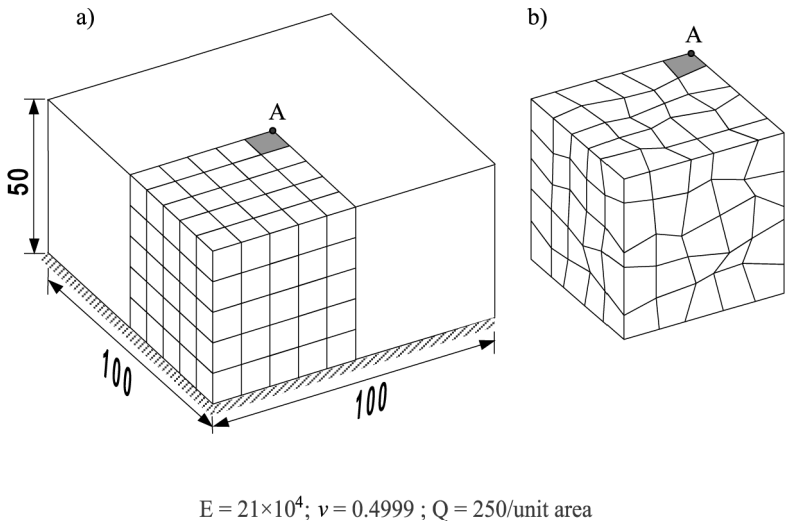

Figure 4. Block with near incompressible properties. (a) Regular mesh, (b) distorted mesh

(Figure 4(a)), and a distorted one (Figure 4(b)). The loaded area is equal for both meshes. The vertical displacement of the central point of the block (A), and the relative error between the solutions for regular and distorted meshes is analysed (Table III).

From the results, it can be inferred that the HCiS12 element is volumetric locking-free, allowing good behaviour in near incompressibility situations, and also having low sensitivity to mesh distortions.

Thick wall sphere problem

This assessment, proposed by Kasper and Taylor (2000), aims to demonstrate the ability of the presented formulations in near incompressible state. One-eighth of a thick walled sphere (Figure 5) with inner radius $R_i = 7.5$ and outer radius $R_e = 10$ is subjected to an internal pressure $Q = 1$. The elastic module is $E = 250$, and the normalized radial displacements for $R = R_e$ is depicted for several Poisson coefficient (ν) values. The HCiS12 and HCiS18 elements results (Table IV) are average values for all nodes with $R = R_e$. The volumetric locking is evident for the Q1 element and the other formulations behave well.

Element	Regular mesh	Distorted mesh	Relative error (per cent)
Q1	1.604×10^{-3}	1.322×10^{-3}	13.15
HCiS12	1.931×10^{-2}	1.927×10^{-2}	0.21
HCiS18	1.913×10^{-2}	1.903×10^{-2}	0.52
QM1/E12[a]	1.892×10^{-2}	1.840×10^{-2}	2.75
QS/E9	1.910×10^{-2}	1.887×10^{-2}	1.20
3D.EAS-21	1.905×10^{-2}	1.830×10^{-2}	3.94

Note: [a]From Korelc and Wriggers (1996).

Table III.
Vertical displacement results in the centre of the block

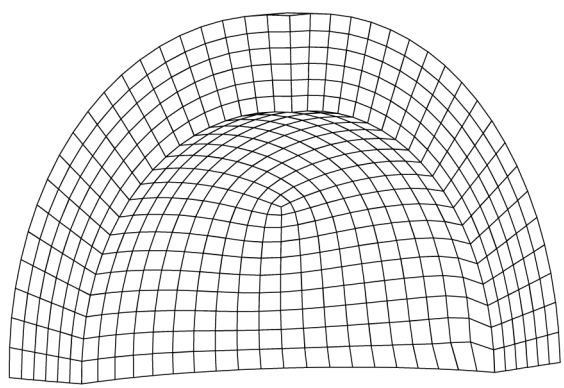

Figure 5.
Thick walled sphere

Morley's 30° skew Plate

This example, originally proposed by Morley (1963), is analysed in order to test the sensitivity of the formulations to mesh distortions and the ability to avoid the shear locking, present in problems with low length to thickness ratio, in this case 1/100. The plate is simply supported and subjected to a uniform pressure Q. The data of the problem, shown in Figure 6, is based on the work of Andelfinger and Ramm (1993).

The Kirchhoff reference solution of 4.455 for the deflection in the center of the plate (C), presented by Morley (1963) is replaced by the value of 4.640 (Andelfinger and Ramm, 1993), since for this thickness to length to ratio of 1/100, the shear deformation effects cannot be neglected.

As can be inferred from Table V and Figure 7, the HCiS12 element shows excellent results even for coarse meshes, being as accurate as the best shell element performance, and showing convergence to the reference solution.

Scordelis-Lo roof problem

The proposed original problem from Scordelis and Lo (1969), reports to a cylindrical shell, with radius R, length L and thickness t, supported by rigid diaphragms in the curved edges and subjected to dead load (Figure 8). Due to its symmetry, only one quarter of the model is studied and the midpoint free edge's vertical displacement (D) is assessed, comparing with the reference solution of 0.3024, from Belytschko *et al.* (1985) and Simo *et al.* (1989).

ν	Q1	HCiS12	HciS18	H1/ME9
0.3	0.998	0.999	0.999	NA
0.49	0.971	0.997	0.998	1.019
0.499	0.782	0.997	0.998	1.001
0.4999	0.268	0.997	0.998	0.999
0.49999	0.004	0.997	0.998	0.999
0.499999	0.006	0.997	0.998	NA
0.4999999	0.001	0.997	0.997	NA

Note: NA – Not available.

Table IV.
Normalized displacements at $R = R_e$ for the thick walled sphere problem

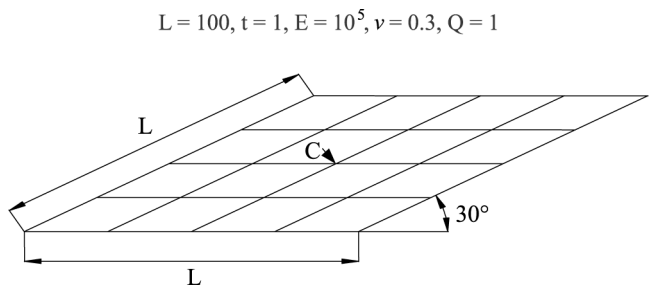

Figure 6.
Morley's 30° skew plate (four elements per side)

Elements per side	4	5	8	9	16	17	32	33
Q1	0.0958	NA	0.3187	NA	0.8165	NA	1.5760	NA
HCiS12	4.5060	NA	4.4210	NA	4.4750	NA	4.5740	NA
HCiS18	4.1000	NA	4.2240	NA	4.3930	NA	4.5340	NA
S4P6E7	4.5090	NA	4.4380	NA	4.4820	NA	4.5610	NA
MITC4[a]	3.9182	NA	3.8991	NA	4.1875	NA	4.4098	NA
EAS7-ANS	4.2122	NA	4.2239	NA	4.3738	NA	4.4827	NA
SIMO_89	NA	4.2820	NA	4.2640	NA	4.3870	NA	4.4960
Reference	4.6400	4.6400	4.6400	4.6400	4.6400	4.6400	4.6400	4.6400

Notes: [a]From Andelfinger and Ramm (1993); NA – not available.

Table V.
Morley's skew plate central point deflection

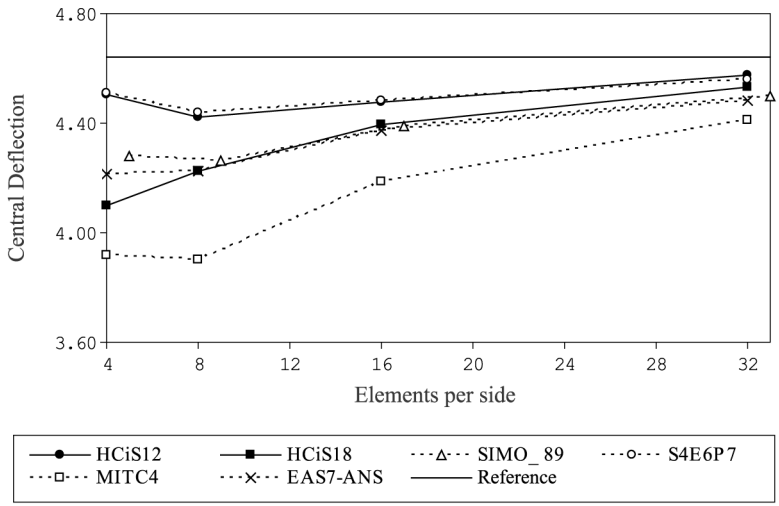

Figure 7.
Central point deflection for Morley's skew plate

The presented results are normalized against the reference solution and represented in Figure 9 and Table VI.

From the results, it can be inferred that all the elements perform well, even for coarse meshes. Besides that, it is important to remark that the solid elements show as good accuracy as the shell elements.

Pinched cylinder with end diaphragms

Figure 10 shows one-eighth of a pinched cylinder with radius R, length L, thickness t and rigid diaphragms at the end edges. The material data are also provided. The structure is subjected to two concentrated loads $F = 1$. This is a classical test for shell elements, and also known for causing poor convergence results in 3D elements. The normalized results for the vertical displacement in the loaded point against the reference solution of 1.82488×10^{-5}, are presented in Table VII, for several distinct meshes, based on the ones used by the authors here in comparison when testing their formulations

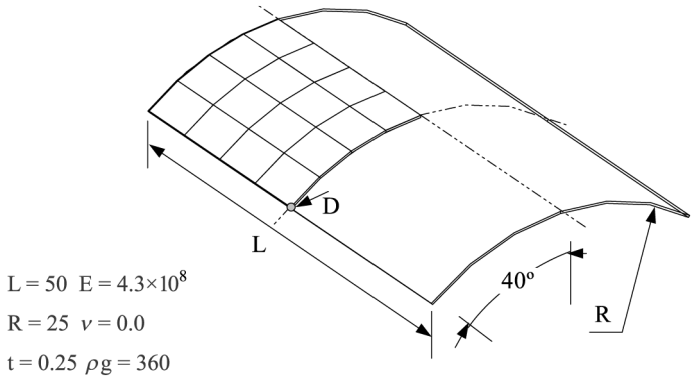

Figure 8.
Scordelis-Lo roof geometry

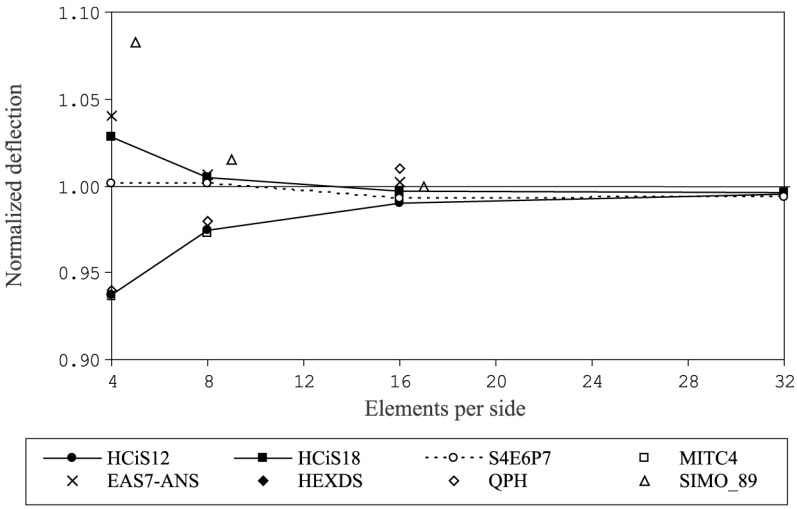

Figure 9.
Scordelis-Lo roof normalized deflection at free edge's midpoint (*D*)

Elements per side	4	5	8	9	16	17	32
HCiS12	0.937	NA	0.974	NA	0.990	NA	0.995
HCiS18	1.028	NA	1.005	NA	0.997	NA	0.996
S4E6P7	1.001	NA	1.002	NA	0.992	NA	0.993
MITC4[a]	0.937	NA	0.973	NA	0.993	NA	NA
EAS7-ANS	1.041	NA	1.006	NA	1.002	NA	NA
HEXDS	NA	NA	1.157	NA	1.137	NA	1.132
QPH	0.940	NA	0.980	NA	1.010	NA	NA
SIMO_89	NA	1.083	NA	1.015	NA	1.000	NA

Notes: [a]From Andelfinger and Ramm (1993); NA – not available.

Table VI.
Scordelis-Lo roof normalized deflection at free edge's midpoint (*D*)

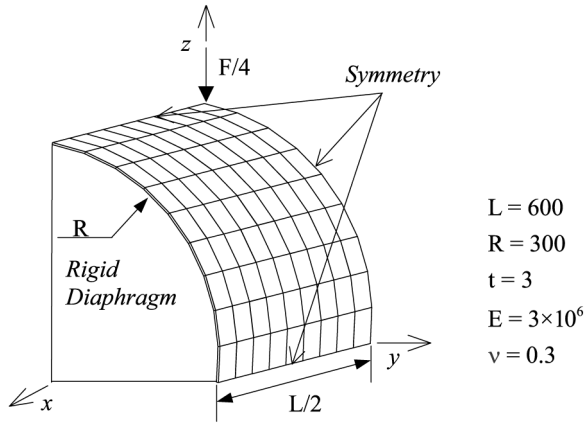

Figure 10.
Pinched cylinder with end diaphragms

Mesh	HCiS12	HCiS18	QS/E9	HEXDS	H1/ME9	QPH	S4E6P7	MITC4[a]	SIMO_89
4 × 4 × 1	0.104	0.106	NA	NA	0.107	0.370	0.392	0.370	NA
5 × 5 × 1	0.188	0.193	0.154	NA	NA	NA	0.514	NA	0.399
8 × 8 × 1	0.494	0.498	NA	NA	0.496	0.740	0.746	0.740	NA
9 × 9 × 1	0.593	0.597	0.506	NA	NA	NA	0.790	NA	0.763
10 × 10 × 2	0.673	0.677	NA	0.801	NA	NA	0.823	NA	NA
16 × 16 × 1	0.912	0.912	NA	NA	0.914	0.930	0.923	0.930	NA
16 × 16 × 4	0.906	0.905	NA	0.945	NA	NA	0.923	NA	NA
17 × 17 × 1	0.928	0.927	0.864	NA	NA	NA	0.932	NA	0.935
20 × 20 × 4	0.950	0.947	NA	0.978	NA	NA	0.969	NA	NA
30 × 30 × 1	0.993	0.987	0.971	NA	NA	NA	0.982	NA	NA
32 × 32 × 1	0.995	0.989	NA	NA	0.992	NA	0.982	NA	NA

Notes: [a]From Belytschko and Leviathan (1994); NA – not available.

Table VII.
Central vertical displacement for the pinched cylinder

for this assessment. The HCiS12 element shows good results and convergence properties, although showing some sensitivity associated with an increase in thickness of elements.

Partly clamped hyperbolic paraboloid

This interesting bending-dominated test was introduced in the work of Chapelle and Bathe (2000) and further developed by Bathe *et al.* (2000). This type of bending-dominated tests can be a hard test for standard FEM formulations. The problem consists of a self-weighted hyperbolic paraboloid shell structure, clamped in one edge, and free in the others, as shown in Figure 11. By symmetry, only one half of the geometry needs to be considered. The geometry details and the problem data can be found in Chapelle and Bathe (2000).

For the FEM meshes, sequences of $N \times N/2$ elements (N = 8, 16, 32, 64) were considered, with thickness/length ratios of 1/100, 1/1,000 and 1/10,000, following the proposal of Bathe *et al.* (2000).

Since there is no analytical solution for this problem, for comparison purposes, the reference values for the vertical displacement of point P and the total strain energy are the ones obtained by Bathe *et al.* (2000) using a high order shell element with a refined mesh. The results present graphically the strain energy error (Er) of the FEM solutions (Eh) against the reference solution (E) (Figures 12-14), i.e.

$$Er = 1 - \frac{Eh}{E} \tag{34}$$

The reference solution is obtained by the solid elements HCiS12 and HCiS18 in all cases, although needing more refined meshes in the last two situations (1/1,000 and 1/10,000), which denotes sensitivity for diminutions in the thickness/length ratio.

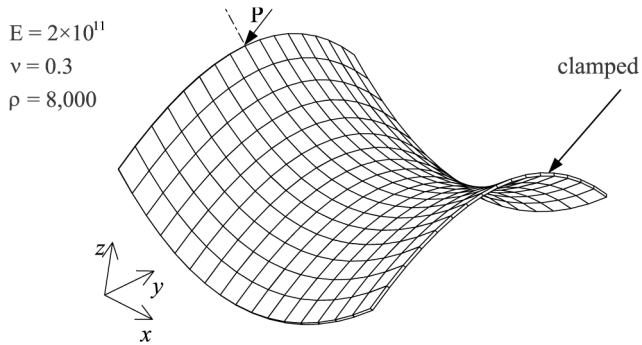

Figure 11.
Hyperbolic paraboloid shell structure

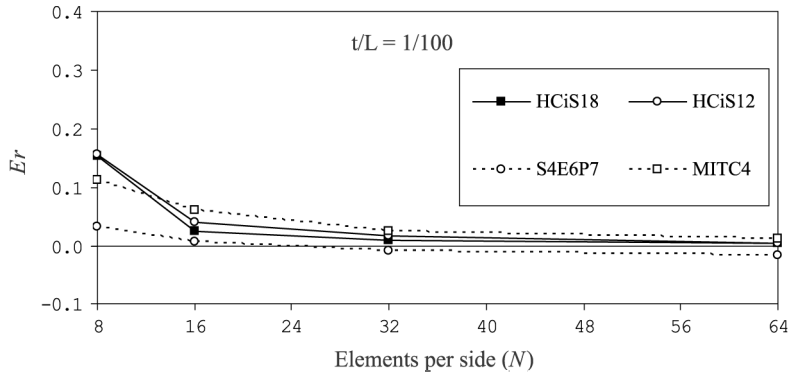

Figure 12.
Relative strain energy error for the hyperbolic paraboloid problem

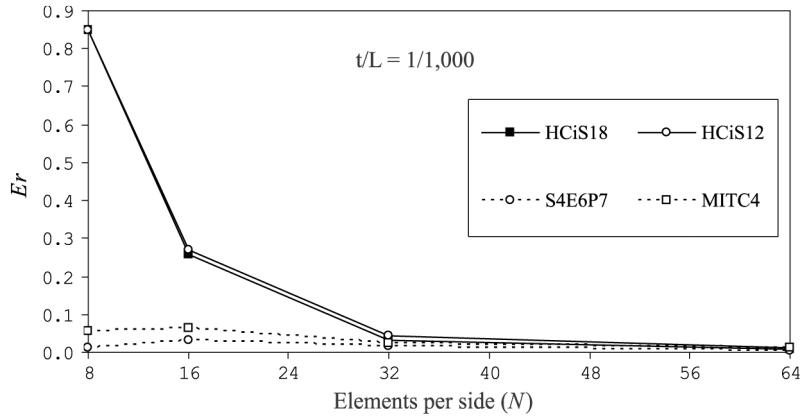

Figure 13.
Relative strain energy error for the hyperbolic paraboloid problem

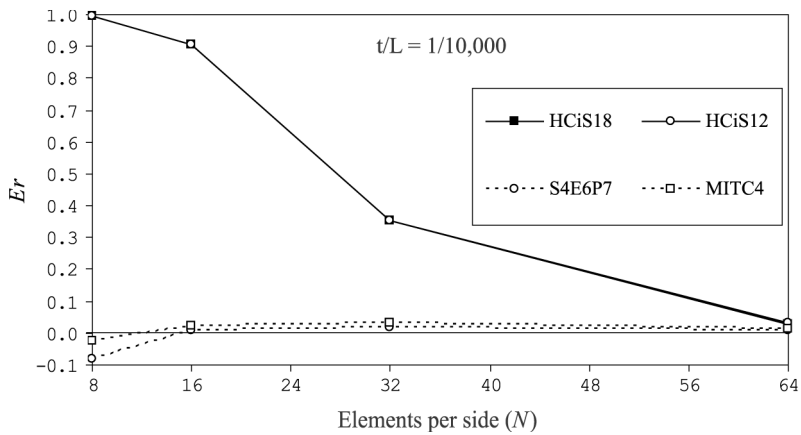

Figure 14.
Relative strain energy error for the hyperbolic paraboloid problem

Concluding remarks

Based on the EAS method, it was possible to design a new eight-noded hexahedral element suited for near incompressible situations and/or thin shell or plate problems. Using a quite simple formulation, with no stabilization or under-integration techniques, and a minimal set of additional variables, justified by the framework of subspace analysis, the HCiS12 element performed successfully in all the examples presented.

- In the block under compression and thick walled sphere examples, no volumetric locking and minimal sensitivity to mesh distortions were seen.
- In the clamped square plate, performed well with low thickness to length ratios allied to near incompressibility.

- In Morley's skew plate, pinched cylinder and Scordelis-Lo roof assessments, the results were excellent for a solid element, showing no shear locking effects.
- In the hyperbolic paraboloid shell, the convergence to correct solutions was achieved, although showing sensitivity related to decrease of the length to thickness ratio from 1/100 to 1/10,000.

Comparing with other well known EAS solid elements, a great improvement was done. The extension of the proposed formulation to geometrically and/or material non-linear problems is currently being carried out.

References

Ahmad, S., Irons, B.M. and Zienkiewicz, O.C. (1970), "Analysis of thick and thin shells structures by curved finite elements", *International Journal for Numerical Methods in Engineering*, Vol. 2, pp. 419-51.

Alves de Sousa, R.J., Natal Jorge, R.M., Areias, P.M.A., Fontes Valente, R.A. and César de Sá, J.M.A. (2002), "Low order elements for 3D analysis", in Mang, H.A., Rammerstorfer, F.G. and Eberhardsteiner, J. (Eds), *Proceedings of the Fifth World Congress on Computational Mechanics (WCCM V)*, 7-12 July, Vienna, Austria, Vienna University of Technology, Austria, ISBN 3-9501554-0-6, http://wccm.tuwien.ac.at

Andelfinger, U. and Ramm, E. (1993), "EAS-Elements for 2D, 3D, plate and shell structures and their equivalence to HR-elements", *International Journal for Numerical Methods in Engineering*, Vol. 36, pp. 1311-37.

Armero, F. and Dvorkin, E.N. (2000), "On finite elements for nonlinear solid mechanics", *Computers and Structures*, Vol. 75 No. 3, Special Issue.

Bathe, K.J. (1996), *Finite Element Procedures*, 2nd ed., Prentice-Hall, New Jersey.

Bathe, K.J. and Dvorkin, E. (1986), "A formulation of general shell elements – the use of mixed interpolation of tensorial components", *International Journal for Numerical Methods in Engineering*, Vol. 22, pp. 697-722.

Bathe, K.J., Iosilevich, A. and Chapelle, D. (2000), "An evaluation of the MITC shell elements", *Computers and Structures*, Vol. 75, pp. 1-30.

Belytschko, T. and Leviathan, I. (1994), "Physical stabilization of the 4-node shell element with one point quadrature", *Computer Methods in Applied Mechanics and Engineering*, Vol. 113, pp. 321-50.

Belytschko, T., Wong, B.L. and Chiang, H.Y. (1992), "Advances in one-point quadrature shell elements", *Computer Methods in Applied Mechanics and Engineering*, Vol. 96, pp. 93-108.

Belytschko, T., Stolarski, H., Liu, W.K., Carpenter, N. and Ong, J.S.J. (1985), "Stress projection for membrane and shear locking in shell finite elements", *Computer Methods in Applied Mechanics and Engineering*, Vol. 51, pp. 221-58.

César de Sá, J.M.A. and Natal Jorge, R.M. (1999), "New enhanced strain elements for incompressible problems", *International Journal for Numerical Methods in Engineering*, Vol. 44, pp. 229-48.

César de Sá, J.M.A. and Owen, D.R.J. (1986), "The imposition of the incompressibility constraint in finite elements – a review of methods with a new insight to the locking phenomena", in Taylor, C., *et al.* (Eds), *Proceedings of the III Internacional Conference on Numerical Methods for Non-Linear Problems*, Dubrovnik, Pineridge Press, Swansea, UK.

César de Sá, J.M.A., Natal Jorge, R.M., Fontes Valente, R.A. and Areias, P.M.A. (2002), "Development of shear locking-free shell elements using an enhanced assumed strain formulation", *International Journal for Numerical Methods in Engineering*, Vol. 53, pp. 1721-50.

Chapelle, D. and Bathe, K.J. (2000), "The mathematical shell model underlying general shell elements", *International Journal for Numerical Methods in Engineering*, Vol. 48, pp. 289-313.

de Borst, R. and Groen, A.E. (1999), "Towards efficient and robust elements for 3D-soil plasticity", *Computers and Structures*, Vol. 70, pp. 23-34.

de Souza Neto, E.A., Peric, D., Dutko, M. and Owen, D.R.J. (1996), "Design of simple low order finite elements for large strain analysis of nearly incompressible solids", *International Journal of Solids and Structures*, Vol. 33, pp. 3277-96.

Doll, S., Schweizerhof, K., Hauptmann, R. and Freischlager, C. (2000), "On volumetric locking of low-order solid and solid-shell elements for finite elastoviscoplastic deformations and selective reduced integration", *Engineering Computations*, Vol. 17, pp. 874-902.

Dvorkin, E.N. and Bathe, K.J. (1984), "A continuum mechanics based four-node shell element for general nonlinear analysis", *Engineering Computations*, Vol. 1, pp. 77-88.

Fontes Valente, R.A., Natal Jorge, R.M., César de Sá, J.M.A. and Areias, P.M.A. (2002), "Application of the enhanced assumed strain concept towards the development of shear locking-free shell elements", in Mang, H.A., Rammerstorfer, F.G. and Eberhardsteiner, J. (Eds), *Proceedings of the Fifth World Congress on Computational Mechanics (WCCM V)*, 7-12 July 2002, Vienna, Austria, Vienna University of Technology, Austria, ISBN 3-9501554-0-6, http://wccm.tuwien.ac.at

Glaser, S. and Armero, F. (1997), "On the formulation of enhanced strain finite elements in finite deformations", *Engineering Computations*, Vol. 14 No. 7, pp. 759-91.

Harnau, M. and Schweizerhof, K. (2002), "About linear and quadratic 'solid-shell' elements at large deformations", *Computers and Structures*, Vol. 80, pp. 805-17.

Hauptmann, R. and Schweizerhof, K. (1998), "A systematic development of 'solid-shell' element formulations for linear and non-linear analyses employing only displacement degrees of freedom", *International Journal for Numerical Methods in Engineering*, Vol. 42, pp. 49-69.

Hauptmann, R., Doll, S., Harnau, M. and Schweizerhof, K. (2001), "Solid-shell elements with linear and quadratic shape functions at large deformations with nearly incompressible materials", *Computers and Structures*, Vol. 79, pp. 1671-85.

Hughes, T.J.R. (1977), "Equivalence of finite elements for nearly incompressible elasticity", *Journal of Applied Mechanics*, Vol. 44, pp. 181-3.

Hughes, T.J.R. (2000), *The Finite Element Method: Linear Static and Dynamic Finite Element Analysis*, 2nd ed., Dover Editions, New Jersey.

Hughes, T.J.R., Cohen, M. and Haroun, M. (1978), "Reduced and selective integration techniques in finite element analysis of plates", *Nuclear Engineering Design*, Vol. 46, pp. 203-22.

Kasper, E.P. and Taylor, R.L. (2000), "A mixed-enhanced strain method: Part I – linear problems", *Computer and Structures*, Vol. 75, pp. 237-50.

Korelc, J. and Wriggers, P. (1996), "An efficient 3D enhanced strain element with Taylor expansion of the shape functions", *Computational Mechanics*, Vol. 19, pp. 30-40.

Lee, P.S. and Bathe, K.J. (2002), "On the asymptotic behaviour of shell structures and the evaluation of finite element solutions", *Computers and Structures*, Vol. 80, pp. 235-55.

Liu, W.K., Guo, Y., Tang, S. and Belytschko, T. (1998), "A multiple-quadrature eight-node hexahedral finite element for large deformation elastoplastic analysis", *Computer Methods in Applied Mechanics and Engineering*, Vol. 154, pp. 69-132.

Morley, L.S.D. (1963), *Skew Plates and Structures*, Pergamon Press, Oxford.

Park, K.C. (1986), "Improved strain interpolation for curved C0 elements", *International Journal for Numerical Methods in Engineering*, Vol. 22, pp. 281-8.

Park, K.C. and Stanley, G. (1986), "A curved C0 shell element based on assumed natural coordinate strains", *Journal of Applied Mechanics*, Vol. 53, pp. 278-90.

Piltner, R. (2000), "An implementation of mixed enhanced finite elements with strains assumed in Cartesian and natural element coordinates using sparse B-matrices", *Engineering Computations*, Vol. 17 No. 8, pp. 933-49.

Rohel, D. and Ramm, E. (1996), "Large elasto-plastic finite element analysis of solids and shells with the enhanced assumed strain concept", *International Journal of Solids and Structures*, Vol. 33, pp. 3215-37.

Scordelis, A.C. and Lo, K.S. (1969), "Computer analysis of cylindrical shells", *Journal of American Concrete Institute*, Vol. 61, pp. 539-61.

Simo, J.C. and Armero, F. (1992), "Geometrically non-linear enhanced strain mixed methods and the method of incompatible modes", *International Journal for Numerical Methods in Engineering*, Vol. 33, pp. 1413-49.

Simo, J.C. and Rifai, M.S. (1990), "A class of mixed assumed strain methods and the method of incompatible modes", *International Journal for Numerical Methods in Engineering*, Vol. 29, pp. 1595-638.

Simo, J.C., Armero, F. and Taylor, R.L. (1993), "Improved versions of assumed enhanced strain tri-linear elements for 3D finite deformation problems", *Computer Methods in Applied Mechanics and Engineering*, Vol. 110, pp. 359-86.

Simo, J.C., Fox, D.D. and Rifai, M.S. (1989), "On a stress resultant geometrically exact shell model", *Computer Methods in Applied Mechanics and Engineering*, Vol. 73, pp. 53-92.

Taylor, R.L., Beresford, P.J. and Wilson, E.L. (1976), "A non-conforming element for stress analysis", *International Journal for Numerical Methods in Engineering*, Vol. 10, pp. 1211-9.

Wilson, E.L., Taylor, R.L., Doherty, W.P. and Ghaboussi, J. (1973), "Incompatible displacement models", in Fenves, S.J., *et al.* (Eds), *Numerical Computational Models in Structural Mechanics*, Academic Press, New York.

Zienkiewicz, O.C. and Taylor, R.L. (2000), *The Finite Element Method*, 5th ed., Butterworth-Heinemann, London.

Zienkiewicz, O.C., Taylor, R.L. and Too, J.M. (1971), "Reduced integration technique in general analysis of plates and shells", *International Journal for Numerical Methods in Engineering*, Vol. 3, pp. 275-90.

Further reading

César de Sá, J.M.A., Areias, P.M.A. and Natal Jorge, R.M. (2001), "Quadrilateral elements for the solution of elasto-plastic finite strain problems", *International Journal for Numerical Methods in Engineering*, Vol. 51, pp. 883-917.

Hughes, T.J.R. (1980), "Generalization of selective integration procedures to anisotropic and nonlinear media", *International Journal for Numerical Methods in Engineering*, Vol. 15, pp. 1413-8.